Large-Scale Molecular Dynamics Study of Entangled Hard-Chain Fluids

Steven W. Smith, Carol K. Hall,* and Benny D. Freeman

Department of Chemical Engineering, North Carolina State University, Raleigh, North Carolina 27695-7905

Equilibrium molecular dynamics is used to simulate fluids comprised of chains of tangent hard spheres. Reptation theory predictions of segmental motion are compared with simulation results. In addition to the usual tube confinement, a second entanglement effect is observed. As the chain disengages from the tube, persistent interchain contacts cause a plateau in the segment mean-square displacement and subsequent accelerated diffusion. Associated with the plateau in the mean-square displacement is a corresponding delay in relaxation of the end-to-end vector as interior chain segments are extended during disentanglement.

PACS numbers: 61.25.Hq, 61.20.Ja, 66.20.+d

Although knowledge of polymer dynamics in the melt state has increased dramatically over the past two decades, detailed information on the molecular motions responsible for observed dynamical behavior is still lacking. In particular, the physical mechanisms responsible for the molecular weight dependence of shear viscosity in the entangled regime are not completely understood because of the following: (1) experiments which access appropriate time and length scales are difficult, and (2) computer simulations that could illuminate these mechanisms have only recently become tractable. We present results from the most extensive computer simulation study to date concerning the dynamics of entangled polymers. By applying efficient algorithms to the simplest model of polymer molecules (the hard-chain model) we have explored large spatial dimensions (192-mers) and long time domains (10^{10} steps). Our results provide new insights regarding the effects of entanglements on polymer diffusion in the long-time limit.

Relative to simple Newtonian liquids, entangled polymer melts contain a rich variety of topological and excluded-volume interactions which create a spectrum of relaxation times. Polymer dynamics are most often discussed in terms of two models: (1) Rouse [1] dynamics for short unentangled chains, and (2) reptation [2] dynamics for highly entangled chains. In the Rouse model, the fluid surrounding a chain relaxes rapidly, providing a stochastic background for a chain's motion. In the reptation model, the surrounding fluid relaxes on an infinite time scale, thus presenting fixed obstacles to a chain's motion.

The tube model of Doi and Edwards [3] is perhaps the most prominent implementation of the reptation concept. In this approach, topological interactions are treated as an effective field of obstacles forming a virtual tube that restricts chain motion. Atomic displacements larger than the characteristic dimension imposed by this field, the so-called tube diameter, occur predominantly along the chain contour. For displacements smaller than the tube diameter, segment motion is restricted only by chain connectivity and should be characterized by Rouse dynamics. Since the longest relaxation time in the Rouse model is

proportional to the chain length squared ($\tau_R \sim N^2$), the tube model predicts that the self-diffusion D and shear viscosity η of short chains scale with molecular weight as $D \sim N^{-1}$ and $\eta \sim N$ in agreement with experiments on short chain melts [4]. When chain length exceeds a critical value, the so-called "entanglement" length, the tube model predicts that the molecular weight scaling for self-diffusion and shear viscosity changes to $D \sim N^{-2}$ and $\eta \sim N^3$. For entangled polymers, the experimentally observed molecular weight dependencies are $D \sim N^{-2}$ and $\eta \sim N^{3.4}$. The discrepancy in viscosity scaling continues to be a recalcitrant problem for molecular theories of polymer dynamics.

Computer simulation offers the advantage of being able to probe the motions of individual molecules, thereby yielding information on the microscopic origins of measurable quantities such as D and η. The first large-scale molecular dynamics (MD) simulations of entangled chains were performed by Kremer and Grest (KG) [5], who applied the Langevin integration technique to polymer chains interacting with a Lennard-Jones site-site potential. Although their results for time-average displacements and internal relaxations agree qualitatively with the predictions of the reptation model, the full spectrum of time dependencies was not examined due to computational limitations.

Polymer molecules in our study are modeled as chains of N freely jointed tangent hard spheres (segments), similar to a pearl necklace. Bond angles between adjacent segments along the chain can take on any value which does not produce intramolecular overlap. This simple model incorporates both chain connectivity, to represent topological constraints, and excluded-volume interactions. The hard-chain simulations are performed using the Rapaport [6] algorithm; the tangency constraint is eliminated by allowing the bond length to vary continuously between $(1 \pm \delta)\sigma$, where δ is 0.1 for all simulations [7]. The simulation develops on an event-by-event basis by locating the next event (segment collision or bond extension) in the system, advancing the system to that point in time, computing the event dynamics, and repeating the process. Neighbor lists,

link lists, and a binary tree for event scheduling [8] yield $(7-15) \times 10^6$ events per CPU hour on our cluster of DEC 3000/300 workstations. Simulation lengths ranged from 10^8 events for the 8-mer fluid to 10^{10} events for the 192-mer fluid; this is about 2 orders of magnitude longer than any previously reported MD simulation.

Simulations were performed on systems containing 32 chains of length $N = 8, 16, 32, 64, 96, 192$ at volume fractions, $\phi \equiv (\pi/6)32N\sigma^3/V$, ranging from 0.3 to 0.45. A cubic simulation cell of volume V was used with normal periodic boundary conditions. Initial configurations were generated by growing each chain from a random walk with a bond length of $1 + \delta/2$. High volume fractions were attained by beginning with a relaxed configuration at a lower volume fraction (e.g., $\phi = 0.3$) and increasing the segment diameter as the simulation proceeded. All configurations were relaxed by moving the chains at least one radius of gyration before production runs. Equilibration was verified by analyzing chain dimensions, fluid structure, and Rouse modes. Self-diffusion coefficients were calculated in the molecular (center-of-mass) reference frame using

$$D^* = \lim_{t\to\infty} \frac{1}{6t^*} \langle |\mathbf{r}_{\text{c.m.}}(t_0 + t) - \mathbf{r}_{\text{c.m.}}(t_0)|^2/\sigma^2 \rangle, \quad (1)$$

where $t^* \equiv t(k_B T/m\sigma^2)^{1/2}$ and $D^* \equiv D/(k_B T/m\sigma^2)^{1/2}\sigma^2$. Uncertainties in D^* were estimated by calculating the standard deviation from two or more independent runs for all systems except for the 192-mers, which required single long runs. The uncertainty for these runs was estimated from the variation in D^* at long times. Although viscosities cannot be calculated easily in equilibrium MD, the end-to-end vector autocorrelation function can be calculated and provides a measure of stress relaxation, and hence, the viscosity [9].

Figure 1 shows the scaling of the reduced self-diffusion coefficient with chain length along with the results from KG. We observe a crossover from Rouse behavior ($D \sim N^{-1}$, solid line) to entangled behavior ($D \sim N^{-2}$, dashed line). The critical chain lengths at which crossover occurs decrease with increasing volume fraction and have values similar to that found by KG. The diffusion coefficients from KG for long chains ($N \geq 150$) are extrapolated values because chain displacement was insufficient to determine D^* directly. Comparison of our D^* values with those from KG for short chain lengths suggests that the volume fraction in the KG simulations is slightly less than 0.45.

The tube model of Doi and Edwards provides scaling predictions for the time dependence of the atomic mean-square displacement (MSD), defined to be $g_1(t) \equiv \langle |r_i(t) - r_i(0)|^2 \rangle$, where $r_i(t)$ is the position of segment i at time t. At short times, when atomic motion is restricted only by chain connectivity, the segments follow Rouse dynamics, that is, $g_1 \sim t^{1/2}$. Once the atomic displacement exceeds the tube diameter a ($t^* = \tau_e$), segments ex-
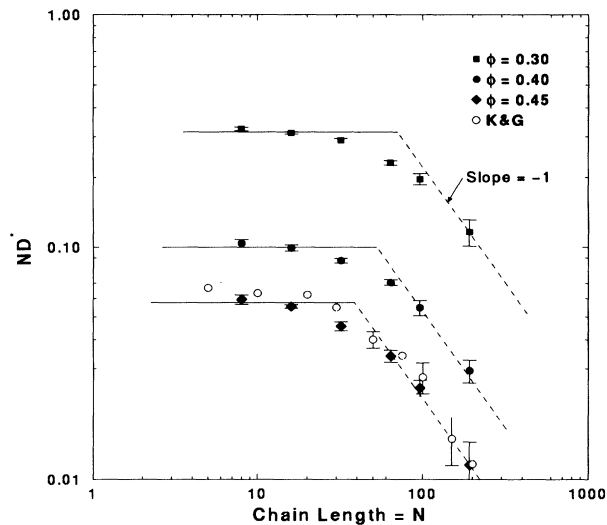

FIG. 1. Simulation results for the reduced self-diffusion coefficient scaled by chain length N versus chain length for three volume fractions. Error bars represent one standard deviation. Data from Kremer and Grest are also shown.

perience Rouse-like relaxation within a virtual tube that is itself a random walk, thus reducing the time dependence to $g_1 \sim t^{1/4}$. As Rouse relaxation is completed ($t^* = \tau_R \sim N^2$), overall chain diffusion along the contour of a rigid tube leads to a third regime with $g_1 \sim t^{1/2}$ that lasts until the tube disengagement time τ_d. However, since the tube in a real polymer melt is not rigid, and instead has a fluctuating contour length [10], tube disengagement is reduced to $\tau_d^{(F)}$, which is estimated [9] to be $\tau_d^{(F)} = \tau_d[1 - 1.3(N_e/N)^{0.5}]^2$, where N_e is the entanglement length. Thus, for chains $5.5N_e$ in length, $\tau_d^{(F)}$ is 20% of the nonfluctuating value τ_d.

MSD analysis is often confined to the inner chain segments [5], because inner chain segment motion should typify the behavior of much longer chains than could be studied via computer simulation. Figure 2(a) compares the time dependence of the MSD for the inner 10 segments of the 192-mer fluid at $\phi = 0.4$ with the MSDs in the atomic and molecular frames of reference. The inner segment and atomic MSDs increase with $t^{1/2}$ at short times, consistent with Rouse behavior as indicated by the dashed line labeled $1/2$. At approximately $t^* = \tau_e = 10^3$, the inner segment MSD begins to deviate from the atomic MSD, exhibiting a scaling of $g_1 \sim t^{0.31}$. A similar analysis for the 192-mer fluid at $\phi = 0.45$ gives a scaling of $g_1 \sim t^{0.28}$, in good agreement with the results of KG and with Monte Carlo studies on long chains confined to a lattice [11]. The decrease in the scaling exponent from 0.31 to 0.28 with increasing density is expected, since tube confinement is more pronounced at higher densities. The reptation prediction $g_1 \sim t^{0.25}$
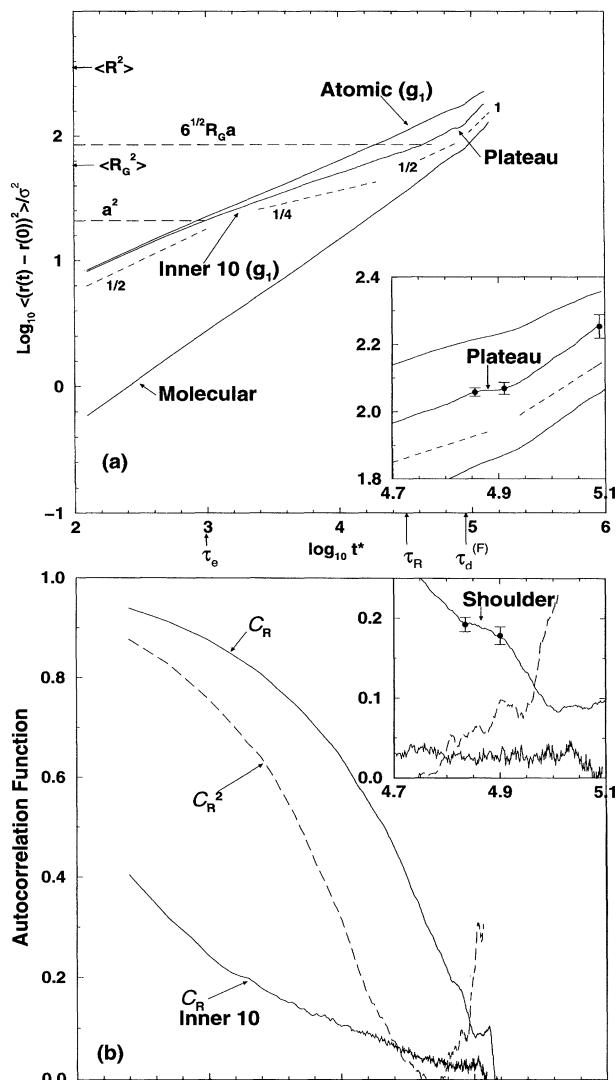
FIG. 2. (a) Mean-square displacement for the atomic, molecular, and inner 10 segments for the 192-mer fluid at $\phi = 0.40$. See text for label explanations. (b) Autocorrelation functions for the orientation (C_R) and magnitude (C_{R^2}) of the end-to-end vector. Insets expand the plateau region and give error bars estimated by averaging over different chains.

could be attained at meltlike volume fractions (estimated to be as high as 0.55 for molten polyethylene [12]). The displacement at the onset of the deviation between the inner segment MSD and the atomic MSD provides an estimate of the tube diameter a and the entanglement time τ_e. From Fig. 2(a) this deviation occurs at $g_1(\tau_e) \approx 20.9\sigma^2$, and since $g_1(\tau_e) = 2\langle R_G^2(N_e)\rangle$ the entanglement length [5] $[N_e = 3g_1(\tau_e)/b^2 + 1]$ is estimated to be 35. The persistence length b is calculated from the chain end-to-end distance and is equal to 1.356σ for $\phi = 0.4$. A similar analysis at $\phi = 0.45$ yields $N_e = 29$.

The third scaling regime predicted by the tube model ($g_1 \sim t^{1/2}$) should occur when the internal Rouse modes of the chain have completely relaxed, $t^* > \tau_R$. An estimate of τ_R can be obtained from the relation [13] $\tau_R/\tau_e = (N/N_e)^2$, which gives $\tau_R = 10^{4.5}$. In addition, the MSD at $t^* = \tau_R$ is related to the tube diameter and radius of gyration [9] R_G by $g_1(\tau_R) = \sqrt{6}R_G a$. These values are consistent with the behavior shown in Fig. 2(a) in that g_1 becomes proportional to $t^{0.55}$ beginning at $t^* = 10^{4.5}$ and ending at $t^* = 10^{4.9}$. If the virtual tube were rigid, this region would persist until $t^* = \tau_d$, or until the MSD were equal to the mean-square end-to-end distance $\langle R^2\rangle$. However, since the 192-mers are only $5.5N_e$ in length, contour length fluctuations reduce the disengagement time to 20% of the nonfluctuating value. Extrapolation of the $t^{0.55}$ region to $\langle R^2\rangle$ gives $\tau_d \approx 10^{5.75}$, which means that $\tau_d^{(F)}/\tau_d = 10^{4.9}/10^{5.75} = 0.16$, in close agreement with the 20% reduction predicted from the relation by Doi.

The most surprising and significant result of these simulations is the appearance of a plateau in the MSD immediately following the $t^{0.55}$ region. This plateau, highlighted in the inset in Fig. 2(a), is not predicted by current theoretical models of polymer dynamics. We attribute this plateau to localized interchain contacts or local knots whose relaxation time exceeds the tube relaxation time $\tau_d^{(F)}$. This interpretation is consistent with the prevailing views of polymer entanglements: (1) that two chains intertwine to form a so-called local "knot" [14], and (2) that surrounding chains form an effective field of obstacles (i.e., tube). Our results suggest that both types of entanglements influence the MSD, but that they occur on different time scales. While the tube model successfully describes many aspects of segmental motion for $t^* < \tau_d$, local knot formation would explain the observed MSD plateau which persists for more than 160×10^6 time steps. MSD analysis for individual chains reveals oscillatory behavior which, upon averaging, gives the observed plateau. These oscillations are indicative of chain motion under the restraint of a localized contact. Such local knots appear to be released only after complete relaxation of the surrounding fluid as dictated by tube decay.

During the MSD plateau, unrestrained sections of the chain continue to experience displacement, and thereby stretch restrained sections beyond their equilibrium or Gaussian separation. This extension of chain sections causes entropic energy to accumulate in the inner segments; when this is released a "superdiffusive" behavior results as inner segment displacement equilibrates with that of the entire chain. Following the plateau phase, the scaling of the inner segment MSD with time is given by $g_1(t) \sim t^{1.12}$. Since the inner segment MSD and atomic MSD must merge in the long-time limit (corresponding to a displacement proportional to $\langle R^2\rangle$), this superdiffu-

sive behavior maintains the appropriate scaling of the self-diffusion coefficient ($D \sim N^{-2}$). The inner segment displacement for the $\phi = 0.45$ case also exhibits a plateau but did not reach the accelerated diffusive regime. Further simulations are in progress to determine the effect of density on the MSD plateau width.

The MSD plateau and subsequent accelerated diffusion also increase the relaxation time for the end-to-end vector autocorrelation function, $C_\mathbf{R} \equiv \langle \mathbf{R}(t) \cdot \mathbf{R}(0) \rangle / \langle R^2 \rangle$. The decay rate of $C_\mathbf{R}$ characterizes the longest relaxation time in the system and is directly correlated to shear viscosity and terminal relaxation time [9]. Figure 2(b) shows $C_\mathbf{R}$ for the 192-mer at $\phi = 0.40$. Simultaneous with the onset of the MSD plateau ($t^* = 10^{4.85}$), a shoulder appears which slows decay in $C_\mathbf{R}$. The source of this shoulder is a persistent plateau in the $C_\mathbf{R}$ of the inner 10 segments [also shown in Fig. 2(b)] originating at the same time. This retarded decay in $C_\mathbf{R}$ indicates that orientational relaxation is impeded during both the MSD plateau and the subsequent superdiffusive regime. A plateau in $C_\mathbf{R}$ could explain the discrepancy between the tube model prediction for shear viscosity and the experimental observation that stress relaxation occurs more slowly for a given molecular weight. Furthermore, storage of entropic energy during the inhibited motion of entangled sections (i.e., stretching) followed by subsequent accelerated motion and release of the stored energy provides a molecular basis for nonlinear rheological behavior such as elastic recovery and normal stresses.

Further evidence for the proposed stretch-release-acceleration mechanism associated with localized knot formation is provided by the autocorrelation function for the magnitude of the end-to-end vector C_{R^2} defined as

$$C_{R^2} \equiv \frac{\langle R^2(t) R^2(0) \rangle - \langle R^2 \rangle^2}{\langle R^4 \rangle - \langle R^2 \rangle^2} . \tag{2}$$

This function characterizes the decay in the magnitude of the largest chain dimension. As presented in Fig. 2(b), C_{R^2} decays to zero at approximately the same time as the plateau region in the MSD. Afterwards, C_{R^2} increases steadily until the beginning of the MSD plateau and then increases more slowly. During the period of accelerated displacement for the inner segments, C_{R^2} again increases rapidly and exhibits a maximum at $t^* = 10^{5.1}$. This oscillatory behavior, indicating memory of previous chain dimensions, is ascribed to chain recoil in a virtual tube after knot release.

In conclusion, we present results from molecular dynamics simulations of entangled chains which cover the longest time domain to date. These simulations are the first to probe atomic displacement in the long-time limit, an accomplishment made possible by judicious model selection coupled with an efficient algorithm and high speed serial computers. Atomic displacements for inner segments experience a period of zero displacement

which is attributed to a localized entanglement formed by interchain contacts or knots. This new scaling region ($g_1 \sim t^0$) in the MSD slows orientational relaxation and could provide a molecular basis for reconciling theoretical predictions with experimental observations on the shear viscosity. Following release of these knots, inner segments of the chain experience accelerated diffusion which maintains the appropriate scaling with respect to chain length for the self-diffusion coefficient. Both the MSD plateau and accelerated diffusion inhibit decay in $C_\mathbf{R}$ and create oscillations in C_{R^2}. Entropic energy stored and released during the stretch and recoil may also explain many nonlinear rheological phenomena for entangled polymers. Simulation results support the tube model for times less than the disengagement time, while at longer times, localized knots become important obstacles to further diffusion. Short video clips extracted from simulation results may be viewed at http://turbo.che.ncsu.edu/smithsw.

*To whom correspondence should be addressed.

[1] P. E. Rouse, J. Chem. Phys. **21**, 1212 (1953).

[2] P. G. de Gennes, *Scaling Concepts in Polymer Physics* (Cornell Univ. Press, Ithaca, NY, 1979).

[3] M. Doi and S. F. Edwards, J. Chem. Soc. Faraday Trans. 2, **74**, 1789 (1978).

[4] G. C. Berry and T. G. Fox, Adv. Polym. Sci. **5**, 261 (1968).

[5] K. Kremer and G. S. Grest, J. Chem. Phys. **92**, 5057 (1990).

[6] D. C. Rapaport, J. Phys. A **11**, L213 (1978); J. Chem. Phys. **71**, 3299 (1979).

[7] S. W. Smith, C. K. Hall, and B. D. Freeman, J. Chem. Phys. **102**, 1057 (1995).

[8] D. C. Rapaport, J. Comput. Phys. **34**, 184 (1980).

[9] M. Doi and S. F. Edwards, *Modern Theory of Polymer Dynamics* (Clarendon, Oxford, 1986).

[10] M. Doi, J. Polym. Sci. Lett. **19**, 265 (1981); Polym. Sci. **21**, 667 (1983).

[11] J. Skolnick, R. Yaris, and A. Kolinski, J. Chem. Phys. **88**, 1401 (1988); J. Phys. Chem. **97**, 3450 (1993).

[12] A. Yethiraj *et al.*, J. Chem. Phys. **98**, 1635 (1993).

[13] W. Paul, K. Binder, D. W. Heerman, and K. Kremer, J. Chem. Phys. **95**, 7726 (1991).

[14] K. Iwata and S. F. Edwards, Macromolecules **21**, 1901 (1988); J. Chem. Phys. **90**, 4567 (1989).

[15] K. L. Ngai and J. Skolnick, Macromolecules **24**, 1561 (1991).